



Oxygen incorporation at the three-phase boundary of LSCF–SDC composite



Bobing Hu, Yunlong Wang, Changrong Xia^{*}

CAS Key Laboratory of Materials for Energy Conversion, Department of Materials Science and Engineering & Collaborative Innovation Center of Suzhou Nano Science and Technology, University of Science and Technology of China, Hefei, Anhui 230026, China

HIGHLIGHTS

- Oxygen incorporation kinetics on LSCF is substantially enhanced with SDC.
- Reaction rate at the LSCF–SDC–gas 3 PB can be quantitatively determined.
- The amount of incorporated oxygen at 3 PB can be quantitatively determined.
- The effective diffusion length of oxygen species on LSCF is about 1.5 μm .

ARTICLE INFO

Article history:

Received 23 January 2014

Received in revised form

29 June 2014

Accepted 30 June 2014

Available online 8 July 2014

Keywords:

Lanthanum strontium cobaltite ferrite

Doped ceria

Composite cathode

Solid oxide fuel cell

Electrical conductivity relaxation

ABSTRACT

Oxygen reduction at LSCF–SDC ($\text{La}_{0.6}\text{Sr}_{0.4}\text{Co}_{0.2}\text{Fe}_{0.8}\text{O}_{3-\delta}$ – $\text{Sm}_{0.2}\text{Ce}_{0.8}\text{O}_{1.9}$) composite cathode might take place at the LSCF–gas two-phase interface (2 PB) and the LSCF–SDC–gas three-phase boundary (3 PB). A method is developed to determine the oxygen incorporation rate and the amount of incorporated oxygen at 3 PB using the electrical conductivity relaxation technique. The obtained results are powerful supports to the viewpoint that oxygen incorporation at 3 PB is much more facile than that at 2 PB. The amount of oxygen incorporated absolutely at 3 PB plays a dominating role in the total process, which actually contributes an average of more than 70% when only 4.5 vol. % SDC is added to LSCF. The incorporation rate at 3 PB is found to be affected not only by the 3 PB length but also the diffusion of oxygen species on the LSCF surface. An effective surface diffusion length of about 1.5 μm is suggested by the relation between the rate, 3 PB length and LSCF surface area.

© 2014 Elsevier B.V. All rights reserved.

1. Introduction

Perovskite oxides based on lanthanum strontium cobalt ferrite (LSCF) are mixed electron-ionic conductors that have potential application in solid-state electrochemical devices such as solid oxide fuel cells (SOFCs) for efficient energy conversion and membrane reactors for clean coal energy delivery. When LSCF is used as the cathode material for SOFC, its ionic conductivity can extend the oxygen reduction sites beyond the electrode–electrolyte interface, to where cathode reaction is limited for the conventional cathode material of lanthanum strontium manganese (LSM), an electronic conductor with negligible ionic conductivity. Although LSCF is an excellent cathode material for SOFCs operated at intermediate-temperatures, its electrochemical performance can be significantly improved by adding a second phase ionic conductor,

typically doped ceria. Dusastre and Kilner have reported that adding 36 vol. % $\text{Gd}_{0.1}\text{Ce}_{0.9}\text{O}_{2-\delta}$ can result in four times lower interfacial polarization resistance for the LSCF cathode [1]. They have further demonstrated that the improvement is consistent with the effective medium percolation theory. Thus, the improved electrochemical performance could be mainly attributed to the increased ionic conductivity of doped ceria. Murray et al. have reported a factor of about 10 decrease in the polarization resistance when 50 vol. % $\text{Gd}_{0.2}\text{Ce}_{0.8}\text{O}_{2-\delta}$ is used as the second phase ionic conductor [2]. They concluded that it seemed likely that the high ionic conductivity of doped ceria played a key role by expanding the electrochemical reaction zone further from the electrode–electrolyte interface. Similar improvements in cathode performance have also been reported by Leng et al. with $\text{Gd}_{0.1}\text{Ce}_{0.9}\text{O}_{2-\delta}$ [3], Fu et al. with $\text{Sm}_{0.2}\text{Ce}_{0.8}\text{O}_{2-\delta}$ [4], and Qiang et al. with $\text{Gd}_{0.2}\text{Ce}_{0.8}\text{O}_{2-\delta}$ [5].

When LSCF is applied for oxygen separation, its mixed conductivity makes it possible to use single-phase LSCF membrane. For example, oxygen permeation flux of about $1.3 \times 10^{-9} \text{ mol s}^{-1} \text{ cm}^{-2}$

^{*} Corresponding author. Tel.: +86 551 63607475; fax: +86 551 63601696.

E-mail address: xiacr@ustc.edu.cn (C. Xia).

is obtained at 800 °C by Shaula et al. with LSCF membrane [6]. The flux could be profoundly improved to $3.2 \times 10^{-8} \text{ mol s}^{-1} \text{ cm}^{-2}$ by adding doped ceria to form a $\text{La}_{0.8}\text{Sr}_{0.2}\text{Fe}_{0.8}\text{Co}_{0.2}\text{O}_{3-\delta}-\text{Ce}_{0.8}\text{Gd}_{0.2}\text{O}_{2-\delta}$ composite membrane. Kharton et al. have also reported that the flux can be improved one order of magnitude higher compared with the single-phase LSCF under the same conditions [7]. They attributed the improvement to the enhanced ionic conductivity by doped ceria based on the comparable fluxes for two composite membranes containing similar volume fractions of LSCF and LSM.

In the literature, the improved performances in both cathode reaction and membrane separation are basically attributed to the enhanced ionic conductivity of doped ceria that accelerates the oxygen bulk diffusion rate. In addition to the bulk diffusion, one should note that the surface reaction plays an important role in the electrochemical processes. Under certain conditions, the surface reaction is the limited step. In the membrane reactor, when the LSCF membrane is thinner than the so-called characteristic thickness, the flux is controlled by the surface step, i.e. further reduce the membrane thickness cannot obviously increase the flux [8]. In SOFC, the surface reaction contributes significantly to the oxygen reduction at LSCF electrode as demonstrated by the electrochemical impedance spectroscopy [9]. At the air sides of SOFCs and oxygen-separation membranes, the surface reaction is oxygen incorporation, which can be written using Kroger–Vink notation as



where $V_{\text{O,LSCF}}^{\bullet\bullet}$ is the oxygen vacancy in LSCF, $\text{O}_{\text{O,LSCF}}^{\times}$ is the crystalline oxygen in LSCF, and e_{LSCF}' is the electron from LSCF. The reaction consists of three steps for single-phase LSCF [10]

Adsorption



Disassociation



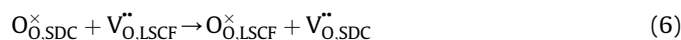
Incorporation



When single-phase LSCF is used, the surface reaction takes place only on the LSCF surface. That is, it takes place at the LSCF–gas two-phase interface (simplified as 2 PB). After adding doped ceria such as $\text{Sm}_{0.2}\text{Ce}_{0.8}\text{O}_{1.9}$ (SDC), the third step (Eq. (4)) may be conducted with oxygen vacancy from SDC, $V_{\text{O,SDC}}^{\bullet\bullet}$



And the oxygen ion transfers to LSCF through bulk diffusion, which has been proved to be very fast through doped ceria [1,2,7].



So, when doped ceria is added, the reaction takes place not only at 2 PB but also at the LSCF–SDC–gas three-phase boundary (3 PB), and possibly, on the doped ceria surface. The reaction at 2 PB is usually characterized with the surface exchange coefficient of LSCF. However, the reaction at 3 PB is not clear yet for any of the LSCF based composites. In this work, a method is presented to characterize the reaction at 3 PB using the electrical conductivity relaxation (ECR) technique. In addition, the contribution from 3 PB is

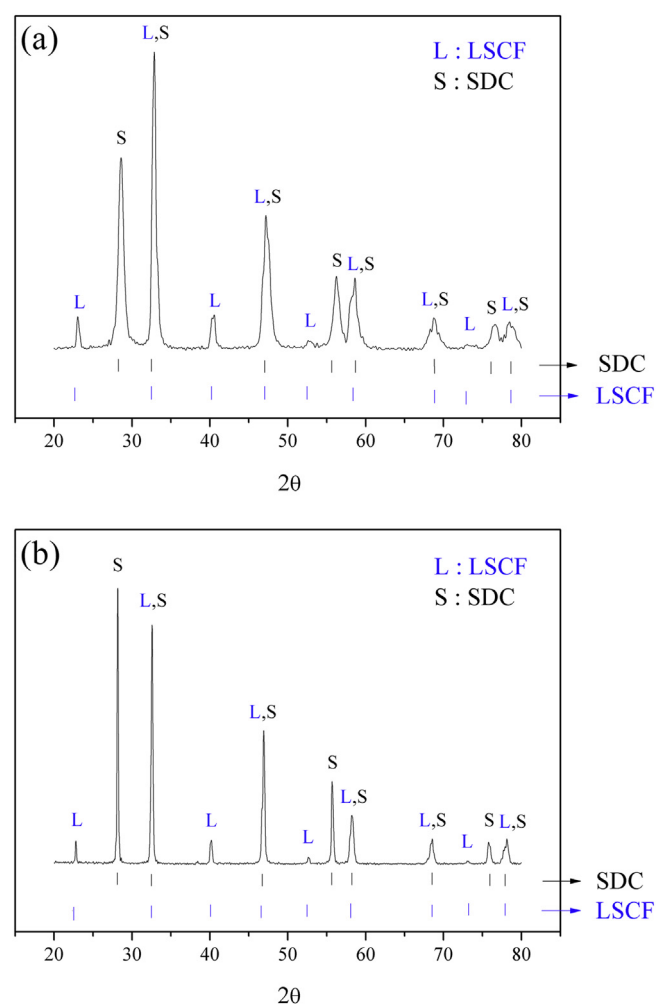


Fig. 1. Room temperature X-ray diffraction pattern of an LSCF–SDC composite (a) before and (b) after sintering at 1500 °C for 5 h. Data from JPCDS PDF #48-0124 (LSCF) and #75-0158 (SDC) is also shown for comparison.

quantitatively determined and discussed with respect to the 3 PB length.

2. Experimental

LSCF ($\text{La}_{0.6}\text{Sr}_{0.4}\text{Co}_{0.2}\text{Fe}_{0.8}\text{O}_{3-\delta}$) powders were synthesized employing conventional solid-state reaction method [11]. La_2O_3 (99.99%), SrCO_3 (99%), Fe_2O_3 (99%) and Co_3O_4 (98%) (Sinopharm Chemical Reagent Co. Ltd) were mixed at the stoichiometric ratio to the nominal composition and then calcined at 1000 °C for 5 h to form LSCF powders with single perovskite structure. Carbonate coprecipitation method was used to prepare the SDC ($\text{Sm}_{0.2}\text{Ce}_{0.8}\text{O}_{1.9}$) powders with $\text{Ce}(\text{NO}_3)_3 \cdot 6\text{H}_2\text{O}$ (99%) and $\text{Sm}(\text{NO}_3)_3 \cdot 6\text{H}_2\text{O}$ (99.95%) as the precursors. The cerium and samarium nitrate solution was dropwise added into a 0.1 mol L^{-1} ammonium carbonate (99%) solution under continuous stirring to form white carbonate precipitates, which were then washed with distilled water and subsequently ethanol three times. The obtained precipitates were dried at 80 °C for 48 h, and then calcined at 600 °C for 2 h to obtain SDC powders with single fluorite structure. All the chemicals were from Sinopharm Chemical Reagent Co. Ltd. The crystal structures of LSCF and SDC powders were identified using X-ray diffractometry (XRD, Philips X'pert PROS diffractometer).

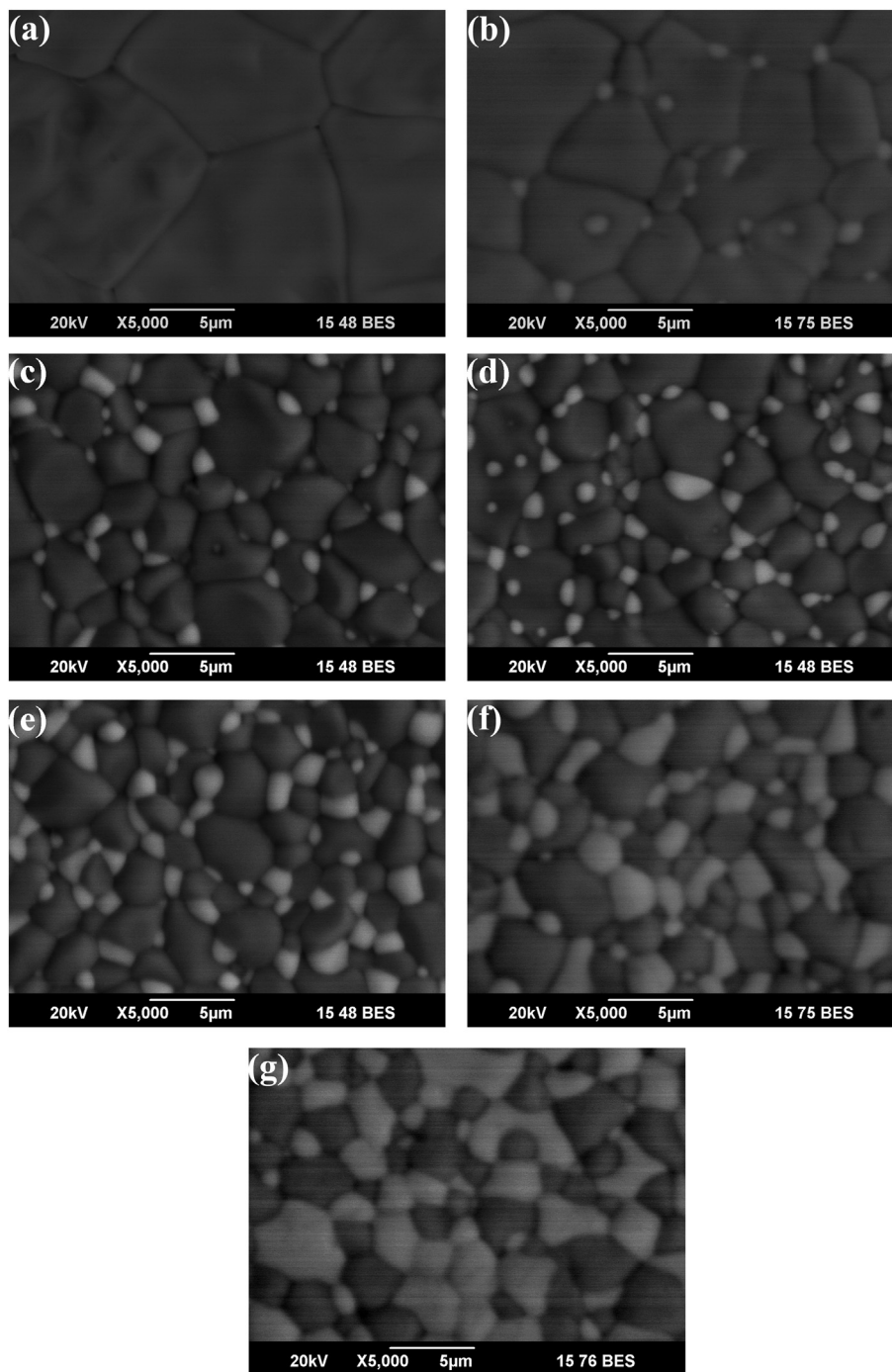


Fig. 2. SEM surface images of LSCF–SDC composites with different SDC volume fractions, f_{V-SDC} = (a) 0, (b) 0.045, (c) 0.091, (d) 0.137, (e) 0.278, (f) 0.424, and (g) 0.575.

Composite powders with SDC weight percentages of 5, 10, 15, 30, 45 and 60% were prepared by mixing and ball milling for 2 h. The corresponding SDC volume fractions were 0.045, 0.091, 0.137, 0.278, 0.424 and 0.575, respectively. The mixed powders were then pressed into rectangular bars at 300 MP and sintered at 1500 °C for 5 h in air to form dense LSCF–SDC samples. The sintered bars had dimensions of $32.00 \times 5.50 \times 0.50 \text{ mm}^3$. The samples were proved to possess a relative density higher than 95% of the theoretical density as determined with the Archimedes method. The microstructure was revealed using scanning electron microscopy (SEM, JSM#6700F). The length of the LSCF–SDC

heterogeneous phase boundary and surface area of both phases were obtained using the image analysis software ImageJ. For each sample, images from at least three different areas of the sample were used to obtain the average values of 3 PB length and surface area.

The incorporation reaction was characterized with the ECR method. The electrical conductivity was measured using the four-probe method with a digital multimeter (Keithley, 2001-785D). Silver wires were used as the lead wires attached to the Ag electrode using silver paste (Sina-Platinum Metals Co. Ltd.) followed by annealing at 600 °C in air for 2 h. The measurement of conductivity

was performed at 800 °C, 750 °C, 700 °C and 650 °C in turn, while the atmosphere was abruptly changed to $P_{O_2} = 0.1$ atm using $O_2 - N_2$ gas mixtures from the initial $P_{O_2} = 0.01$ atm after reaching the equilibration at each temperature. And the gas switches were realized in less than 1 s at a gas-flow rate of 300 ml min⁻¹.

3. Results and method

3.1. Microstructure characteristics

Fig. 1 shows the XRD pattern of the LSCF–SDC composite with 42.4 vol. % SDC before and after sintering at 1500 °C for 5 h. The standard peaks of perovskite LSCF and fluorite SDC are also shown according to the JPCDS PDF #48-0124 and #75-0158, respectively. The peak intensity and width have been changed by the sintering process. The reduced width suggests grain-growth as the result of high temperature sintering. And the change in relative intensity may be attributed to factors such as the orientation of the grain throughout the sintering process. No impurity phases are found, suggesting no obvious solid-state reaction occurs between LSCF and SDC under the conditions to fabricate the dense samples. Similar results are reported by Kharton et al. [7], who have fabricated dense LSCF-GDC (50:50 wt. %) membranes via sintering at 1500 °C for 2 h.

Fig. 2 shows the backscattered electron SEM images of the LSCF–SDC composites with different SDC contents. It is clear that the samples are completely dense. The brighter part represents SDC phase for its bigger molecular weight, while the dark part is LSCF phase. The two-phase boundary is very distinct, further suggesting no solid-state reaction occurs in the boundary region. It is worth mentioning that the grain growth of LSCF phase has been significantly inhibited owing to the addition of SDC phase. The average grain sizes of LSCF and SDC are counted and listed in Table 1. The length of 3 PB per unit area, L_{3PB} (cm⁻¹), and the area fraction of SDC, f_{S-SDC} , is quantificationally counted with the image analysis software ImageJ. The results are shown in Table 1 and Fig. 3. The maximum 3 PB length is observed at $f_{V-SDC} = 0.424$, where f_{V-SDC} is SDC volume fraction. The SDC surface fraction increases surely with its volume fraction.

3.2. Oxygen incorporation on single-phase LSCF

There are several reports on the ECR method for oxygen incorporation on single-phase material such as LSCF [12,13]. The method is addressed here in a different manner to clearly present our approach for the LSCF–SDC dual-phase composites.

3.2.1. Incorporation rate and the amount of incorporated oxygen

When the oxygen partial pressure in the gas phase increases from $P_{O_2} = 0.01$ to 0.1 atm, oxygen incorporates to LSCF till a new thermodynamic equilibrium state is reached. The incorporation increases the oxygen ionic concentration, and consequently,

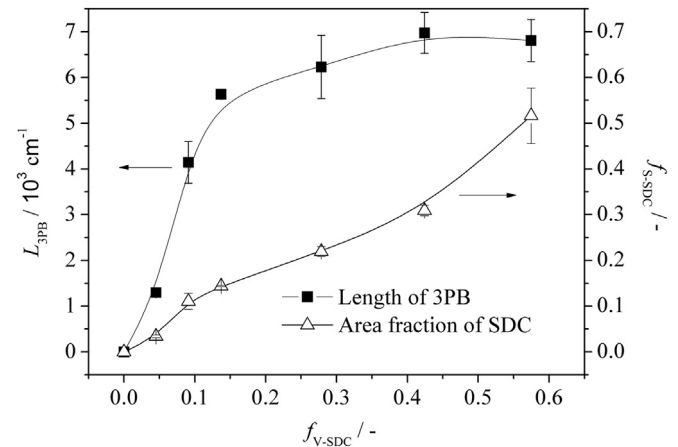


Fig. 3. Length of 3 PB per unit area, L_{3PB} , and SDC area fraction, f_{S-SDC} , as a function of SDC volume fraction, f_{V-SDC} .

changes the electrical conductivity. With a linear assumption between the conductivity and concentration [14], the following equation is derived

$$n(t) = \frac{\sigma(t) - \sigma(0)}{\sigma(\infty) - \sigma(0)} = \frac{c(t) - c(0)}{c(\infty) - c(0)} \quad (7)$$

where $n(t)$ is the dimensionless, normalized change in the conductivity/concentration, $c(t)$ (mol cm⁻³) and $\sigma(t)$ (S cm⁻¹) are, respectively, the concentration and conductivity at time t , $c(0)$ and $\sigma(0)$ the corresponding initial values, $c(\infty)$ and $\sigma(\infty)$ those at infinite time (i.e. equilibrium time/relaxation time) when the new thermodynamic equilibrium state is achieved.

Fig. 4a is the normalized concentration/conductivity, $n(t)$, versus the incorporation time measured at 700 °C. The profile is typical for the ECR measurement. The absolute amount of incorporated oxygen per unit surface area of the sample, $H_{2PB}(t)$ (mol cm⁻²), which is incorporated to LSCF at 2 PB, is

$$H_{2PB}(t) = \frac{V[c(t) - c(0)]}{S} = \frac{V}{S} [c(\infty) - c(0)] n(t) \quad (8a)$$

where V (cm³) is the bulk volume, and S (cm²) is the surface area of the bar sample exposed to the gas phase. Fig. 4b shows that $H_{2PB}(t)$ increases with the relaxation time, the curve has the exactly same shape with Fig. 4a. The value of $c(\infty) - c(0)$ is constant for a given step change in P_{O_2} and at a fixed temperature, and may be calculated from the oxygen nonstoichiometry, δ , in $La_{0.6}Sr_{0.4}Co_{0.2}Fe_{0.8}O_{3-\delta}$, where δ is a function of P_{O_2} and temperature. For example, at 700 °C, $c(\infty) - c(0)$ is about 5×10^{-4} mol cm⁻³ for LSCF when P_{O_2} is changed from 0.01 to 0.1 atm [15]. The relative amount of incorporated oxygen per unit surface area, $h_{2PB}(t)$, is then defined

Table 1
Microstructure characteristics of the LSCF–SDC composites.

SDC volume fraction/-	SDC surface fraction/-	LSCF particle size/10 ⁻⁴ cm	SDC particle size/10 ⁻⁴ cm	Sample thickness/10 ⁻² cm	Length of 3 PB per unit area/10 ³ cm ⁻¹
0	0	12.15 ± 1.26	0	4.9 ± 0.2	0
0.045	0.034 ± 0.003	4.72 ± 0.38	0.61 ± 0.03	5.0 ± 0.2	1.30 ± 0.04
0.091	0.111 ± 0.017	3.54 ± 0.45	0.74 ± 0.08	4.9 ± 0.1	4.14 ± 0.45
0.137	0.144 ± 0.002	3.12 ± 0.04	0.83 ± 0.02	4.7 ± 0.3	5.63 ± 0.05
0.278	0.220 ± 0.011	2.96 ± 0.23	1.11 ± 0.09	5.0 ± 0.2	6.23 ± 0.69
0.424	0.309 ± 0.011	2.85 ± 0.14	1.73 ± 0.10	5.0 ± 0.1	6.98 ± 0.44
0.575	0.516 ± 0.060	2.53 ± 0.23	2.68 ± 0.21	4.9 ± 0.2	6.80 ± 0.46

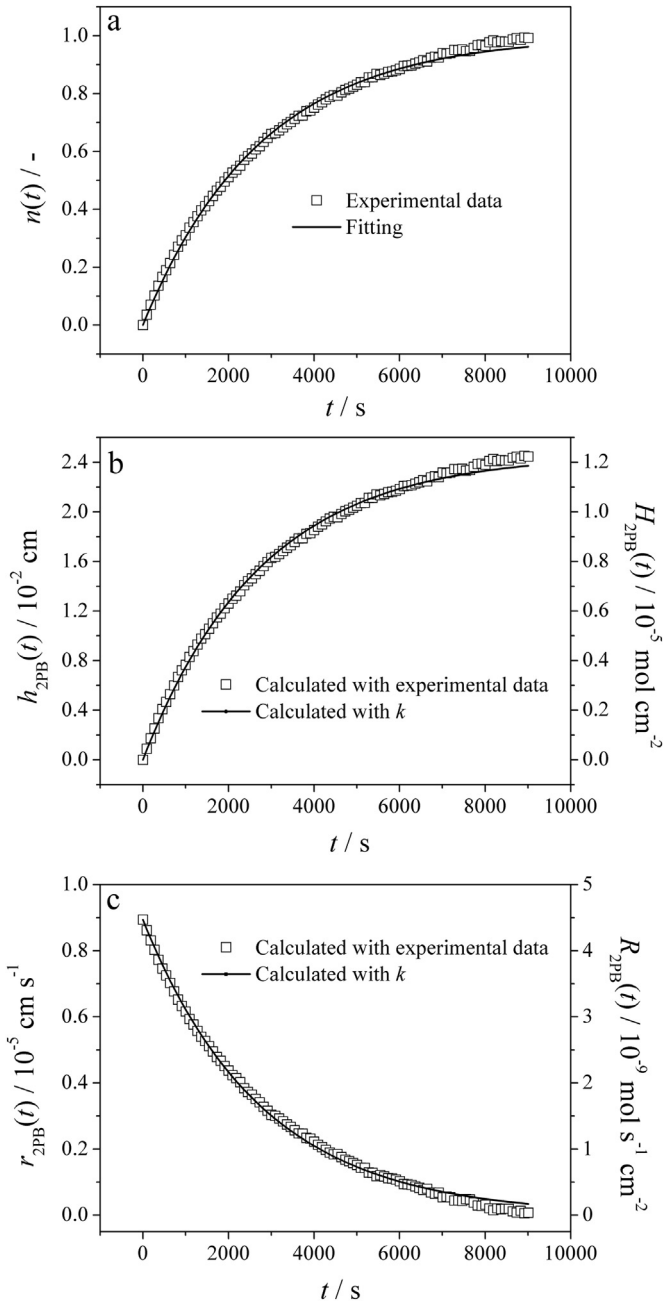


Fig. 4. a) The normalized conductivity, $n(t)$, b) the amount of incorporated oxygen, $H_{2PB}(t)$ and $h_{2PB}(t)$, and c) the incorporation rate, $R_{2PB}(t)$ and $r_{2PB}(t)$, as a function of the relaxation time for single-phase LSCF sample at 700 °C. The open symbols represent the data derived directly from the experimental results while the lines are the results calculated with k under the assumption that the incorporation is controlled by the surface step.

$$h_{2PB}(t) = \frac{H_{2PB}(t)}{[c(\infty) - c(0)]} = \frac{V}{S} n(t) \quad (8b)$$

$h_{2PB}(t)$ (cm) is used instead of $H_{2PB}(t)$, for convenience, to represent the amount of incorporated oxygen per unit surface area in the relaxation process at different temperatures. When the incorporation process reaches a new thermodynamic equilibrium state, the reaction stops. Thus, $H_{2PB}(\infty)$ and $h_{2PB}(\infty)$ mean the total amount of the incorporated oxygen per unit surface area.

The absolute oxygen incorporation rate per unit surface area, $R_{2PB}(t)$ ($\text{mol s}^{-1} \text{cm}^{-2}$), can be subsequently obtained with $H_{2PB}(t)$

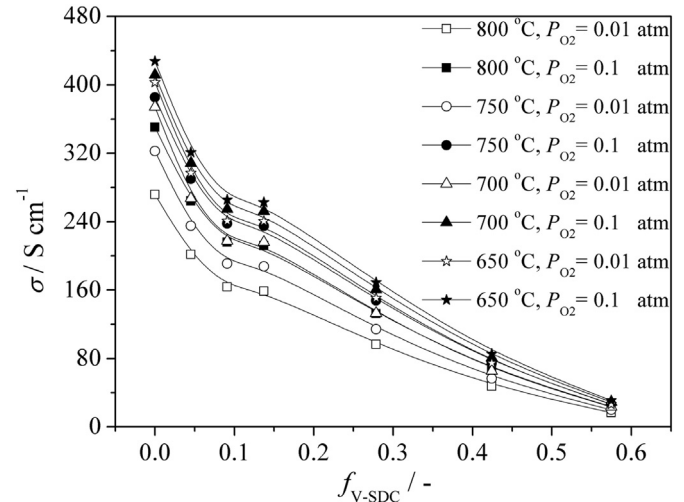


Fig. 5. Conductivities at various temperatures for LSCF–SDC composites as a function of SDC volume fraction.

$$R_{2PB}(t) = \frac{\partial H_{2PB}(t)}{\partial t} = \frac{V}{S} [c(\infty) - c(0)] \frac{\partial n(t)}{\partial t} \quad (9a)$$

Fig. 4c shows that $R_{2PB}(t)$ decreases exponentially with time. The relative oxygen incorporation rate per unit surface area, $r_{2PB}(t)$ (cm s^{-1}), is defined as

$$r_{2PB}(t) = \frac{R_{2PB}(t)}{[c(\infty) - c(0)]} = \frac{V}{S} \frac{\partial n(t)}{\partial t} \quad (9b)$$

$r_{2PB}(t)$ is used instead of $R_{2PB}(t)$ to represent the oxygen incorporation rate per unit surface area at 2 PB. Direct comparing the incorporation rate at any moment is complex and meaningless since the oxygen ion concentration changes with time, Fig. 4a. However, at the right moment when the incorporation proceeds ($t = 0$ s), the rate, $r_{2PB}(0)$, is the highest while the oxygen concentration remains the initial value. That is, $r_{2PB}(0)$ is caused by the highest concentration difference of $c(\infty) - c(0)$, which corresponds to $P_{O_2} = 0.1$ atm and 0.01 atm, respectively. Thus, $r_{2PB}(0)$ is used to compare the incorporation rate.

3.2.2. Incorporation and surface exchange coefficient

The incorporation comprises two sequential steps, which are oxygen reduction on the surface (Eqs. (3) and (4)) and bulk diffusion within the oxide. The diffusion step is controlled by the bulk diffusion coefficient, D ($\text{cm}^2 \text{s}^{-1}$), and the length to diffuse. When the sample is thin enough, which often means its thickness is smaller than the characteristic thickness, the diffusion step is so fast that the incorporation reaction is limited only by the surface step. For LSCF in this work, the reaction is limited by the surface step since its diffusion thickness is 0.25 mm, much less than its characteristic thickness, which is about 1.5 mm at 700 °C [16]. In this case, the incorporation rate at 2 PB can be directly derived from the chemical surface exchange coefficient, k (cm s^{-1}), which is determinable with the ECR method using much simple equations to fit the time-dependent conductivity curve as shown in Fig. 4a [17,18].

$$\frac{\partial c(t)}{\partial t} = -\frac{S}{V} k [c(t) - c(\infty)] \quad (10)$$

Integration of Eq. (10) gives the relative change of the oxygen concentration as a function of time

$$n(t) = \frac{c(t) - c(0)}{c(\infty) - c(0)} = 1 - \exp\left(-\frac{S}{V}kt\right) \quad (11)$$

The experimental result is fitted with the surface exchange controlling E exponential function (Eq. (11)). And the fitting line is also shown in Fig. 4a. The fitting result matches well with the experimental data with adj. R square over 0.99. The exchange coefficient, k , at 700 °C is calculated to be $0.89 \times 10^{-5} \text{ cm s}^{-1}$, which agrees well with the previous result, $0.7 \times 10^{-5} \text{ cm s}^{-1}$, reported by Bouwmeester et al. [19]. With the k value, the amount of incorporated oxygen per unit surface area at 2 PB can be obtained by combining Eq. (8) (a, b) and Eq. (11)

$$h_{2PB}(t) = \frac{V}{S} \left[1 - \exp\left(-\frac{S}{V}kt\right) \right] \quad (12)$$

When the surface step limits the incorporation reaction, the oxygen incorporation rate per unit surface area can be directly obtained with k using Eq. (13) [14]

$$r_{2PB}(t) = k \exp\left(-\frac{S}{V}kt\right) \quad (13)$$

$H_{2PB}(t)$, $h_{2PB}(t)$, $R_{2PB}(t)$ and $r_{2PB}(t)$ calculated with k are also shown in Figs. 4b and c. The values calculated with k match well with the experimental results.

3.3. Oxygen incorporation on LSCF–SDC dual-phase composite

3.3.1. Conductivity relaxation of LSCF–SDC composite

In the LSCF–SDC composite, LSCF is a mixed electronic-ionic conductor while SDC is an ionic conductor. The SDC conductivity is about 0.05 S cm^{-1} at 700 °C [20], about four magnitudes lower than LSCF, which is nearly 400 S cm^{-1} measured in this work. Fig. 5 illustrates the composite conductivity. It is obvious that the conductivity decreases with SDC volume fraction. The conductivity in $P_{O_2} = 0.1 \text{ atm}$ atmosphere is higher than that containing 1% O_2 due to the p-type conductivity of LSCF. In an oxidizing atmosphere, $P_{O_2} > 10^{-3} \text{ atm}$, the oxygen stoichiometry of SDC hardly varies with P_{O_2} and, hence, the associated conductivity will be virtually constant [20]. Consequently, when ECR measurement is conducted on the LSCF–SDC composite, the conductivity change is solely associated with the LSCF phase.

Fig. 6a shows the relaxation profiles at 700 °C for the composites with different SDC contents. Fig. 6b shows the curves for $t < 2000 \text{ s}$ to clear compare the compositional effect. The relaxation curves are very similar to the single-phase LSCF, suggesting that the oxygen incorporation process for the composite is basically the same as that for the single-phase LSCF. The relaxation time, $t(\infty)$, is effectively reduced by adding SDC. It is more than 9000 s for the single-phase LSCF, reduced to 3600 s when 4.5 vol. % SDC is added, and to the lowest of 2800 s for the composite with 13.7 vol. % SDC.

3.3.2. Incorporation rate and the amount of incorporated oxygen

Using the same method for the single-phase LSCF, the amount of incorporated oxygen per unit surface area of the composite sample, $h_c(t)$, and the corresponding incorporation rate per unit surface area, $r_c(t)$, for the LSCF–SDC composite can be derived via

$$h_c(t) = f_{V-LSCF} \frac{V}{S} n_c(t) \quad (14)$$

$$r_c(t) = f_{V-LSCF} \frac{V}{S} \frac{\partial n_c(t)}{\partial t} \quad (15)$$

where $n_c(t)$ is the normalized oxygen concentration change of LSCF in the composite, and f_{V-LSCF} is the LSCF volume fraction in the

composite. The results are shown in Fig. 7a and b for the typical composite with 42.4 vol. % SDC at 700 °C.

3.3.3. Incorporation and the effective surface exchange coefficient

For the single-phase LSCF, the amount of incorporated oxygen and the incorporation rate per unit surface area can be directly obtained with the surface exchange coefficient, Eqs. (12) and (13). Analogically, $H_c(t)$, $h_c(t)$, $R_c(t)$ and $r_c(t)$ can be obtained using a so-called effective oxygen surface exchange coefficient, k_{eff} (cm s^{-1}), which is defined for the composite by assuming that the surface reaction takes place homogeneously on the overall surface of the LSCF–SDC composite. k_{eff} can be determined by fitting the experimental data. That is,

$$n_c(t) = \frac{c_c(t) - c(0)}{c(\infty) - c(0)} = 1 - \exp\left(-\frac{S}{Vf_{V-LSCF}}k_{\text{eff}}t\right) \quad (16)$$

where $c_c(t)$ (mol cm^{-3}) is the oxygen concentration at time t in the LSCF phase. Fig. 6 also shows the fitting lines, which agree well with the experimental results. Fig. 8 compares the effective oxygen surface exchange coefficients at various SDC volume fractions. A marked enhancement in the surface exchange coefficient is readily observed when SDC is added, suggesting the incorporation rate is greatly improved by SDC.

Similar with the approach used for the single-phase LSCF, $h_c(t)$ and $r_c(t)$ can be calculated with k_{eff} .

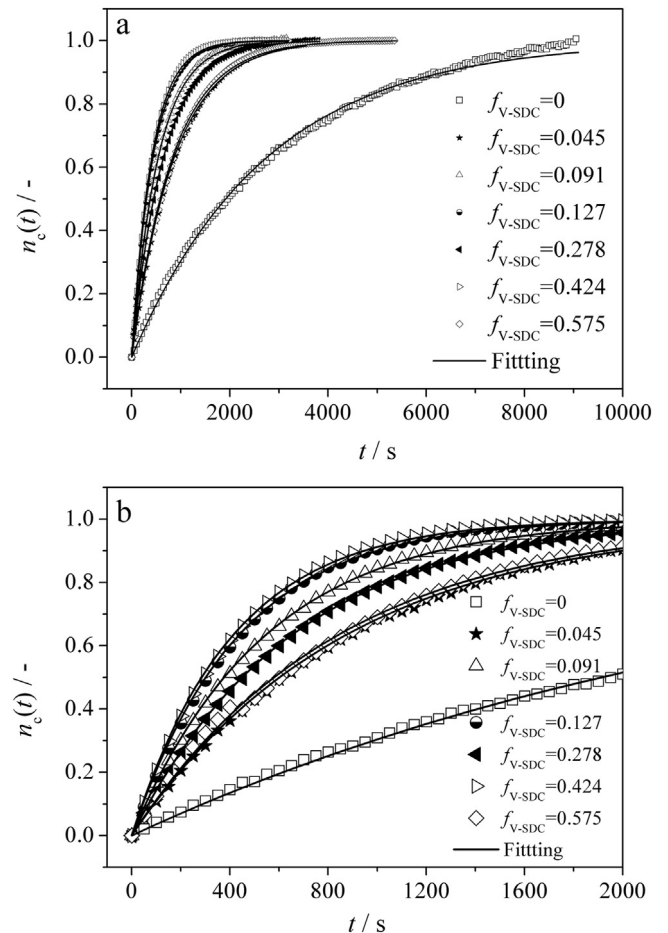


Fig. 6. Normalized conductivities, $n_c(t)$, for LSCF–SDC composites with different SDC volume fractions. The lines are the fitting results.

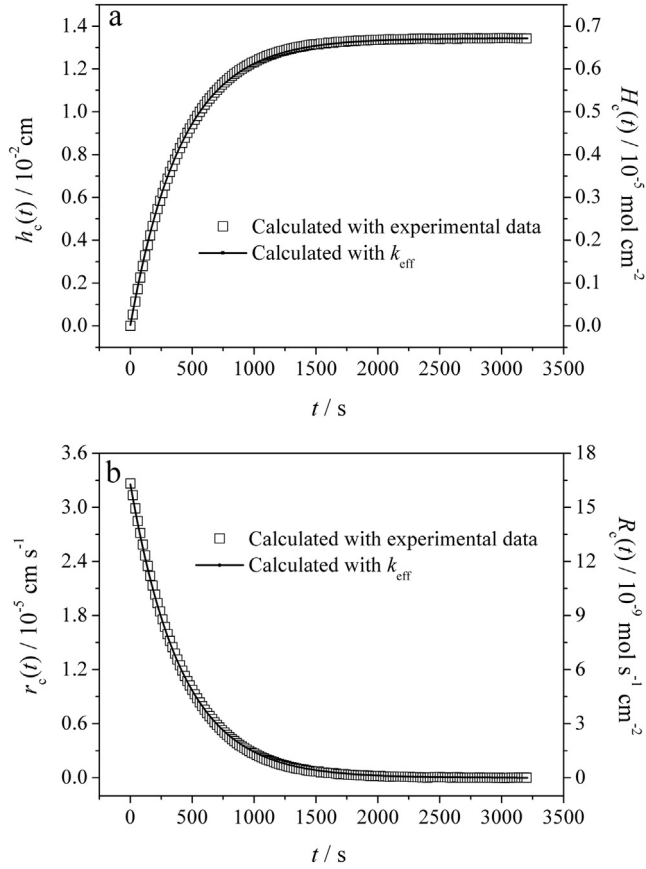


Fig. 7. a) The amount of incorporated oxygen, $H_c(t)$ and $h_c(t)$, and b) the incorporation rate, $R_c(t)$ and $r_c(t)$, for the composite with 42.4 vol. % SDC as a function of the relaxation time at 700 °C. The open symbols represent the data derived directly from the experimental results while the lines are the results calculated with k_{eff} .

$$h_c(t) = f_{V-\text{LSCF}} \frac{V}{S} \left[1 - \exp\left(-\frac{S}{V f_{V-\text{LSCF}}} k_{\text{eff}} t\right) \right] \quad (17)$$

$$r_c(t) = k_{\text{eff}} \exp\left(-\frac{S}{V f_{V-\text{LSCF}}} k_{\text{eff}} t\right) \quad (18)$$

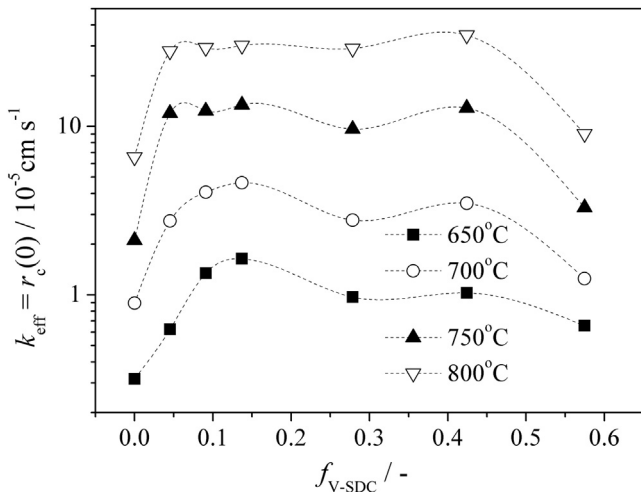


Fig. 8. Effective exchange coefficient, k_{eff} /The initial incorporation rate, $r_c(0)$, versus SDC volume fraction. Dashed lines are drawn to guide the eye.

Fig. 7a and b also show the amount of exchanged oxygen and the incorporation rate per unit surface area as calculated with k_{eff} , respectively. Fig. 8 indicates the initial incorporation rate per unit surface area, $r_c(0)$, which is equal to k_{eff} as shown by Eq. (18). Fig. 9 shows the total amount of incorporated oxygen per unit surface area, $h_c(\infty)$, for the composites with different SDC contents. The total amount of incorporated oxygen decreases linearly with the increase of SDC volume fraction. The fitting line shows that when $f_{V-\text{SDC}} = 1$, $h_c(\infty) \approx 0$, demonstrating that SDC does not take part in the relaxation process.

3.4. Oxygen incorporation at LSCF–SDC–gas 3 PB

3.4.1. Incorporation rate at 3 PB

The oxygen incorporation on the LSCF–SDC dual-phase composite surface is quite different with that on the single-phase LSCF. The incorporation must take place at any of the following three sites: the SDC–gas two-phase interface, the LSCF–gas two-phase interface (2 PB), and the LSCF–SDC–gas three-phase boundary (3 PB). It is noted that the oxygen surface exchange coefficient for the single-phase SDC is very low, $\sim 10^{-8} \text{ cm s}^{-1}$ at 750 °C [21]. It is about three orders of magnitude lower than that for LSCF, $2.11 \times 10^{-5} \text{ cm s}^{-1}$, under the similar conditions. Thus, the contribution from the SDC–gas interface can be neglected. Consequently, the incorporation must occur at either 2 PB or 3 PB. And the reaction rate should be the sum of the rates at 2 PB and 3 PB. At the right moment when the incorporation starts, the rate at 2 PB per unit surface area of the LSCF–SDC composite sample is

$$r_{2\text{PB},c}(0) = r_{2\text{PB}}(0) f_{S-\text{LSCF}} \quad (19)$$

where $f_{S-\text{LSCF}}$ is the LSCF area fraction in the composite. And

$$r_{3\text{PB}}(0) = r_c(0) - r_{2\text{PB},c}(0) \quad (20)$$

Thus, the starting rate at 3 PB can be experimentally determined. Fig. 10a shows the starting rate versus SDC volume fraction. Once the reaction proceeds, the incorporation rate cannot be obtained from an equation similar to Eq. (19) since $n(t)$ is different with $n_c(t)$. It can be obtained with k since the reaction is limited by the surface step.

$$r_{2\text{PB},c}(t) = \frac{f_{S-\text{LSCF}} k [c(\infty) - c_c(t)]}{c(\infty) - c(0)} \quad (21)$$

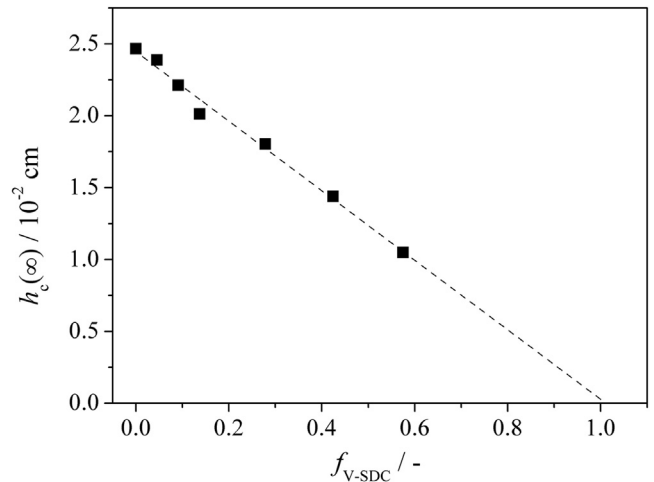


Fig. 9. The total amount of incorporated oxygen per unit surface area of LSCF–SDC composite versus SDC volume fraction. The dashed line represents the linear fitting result.

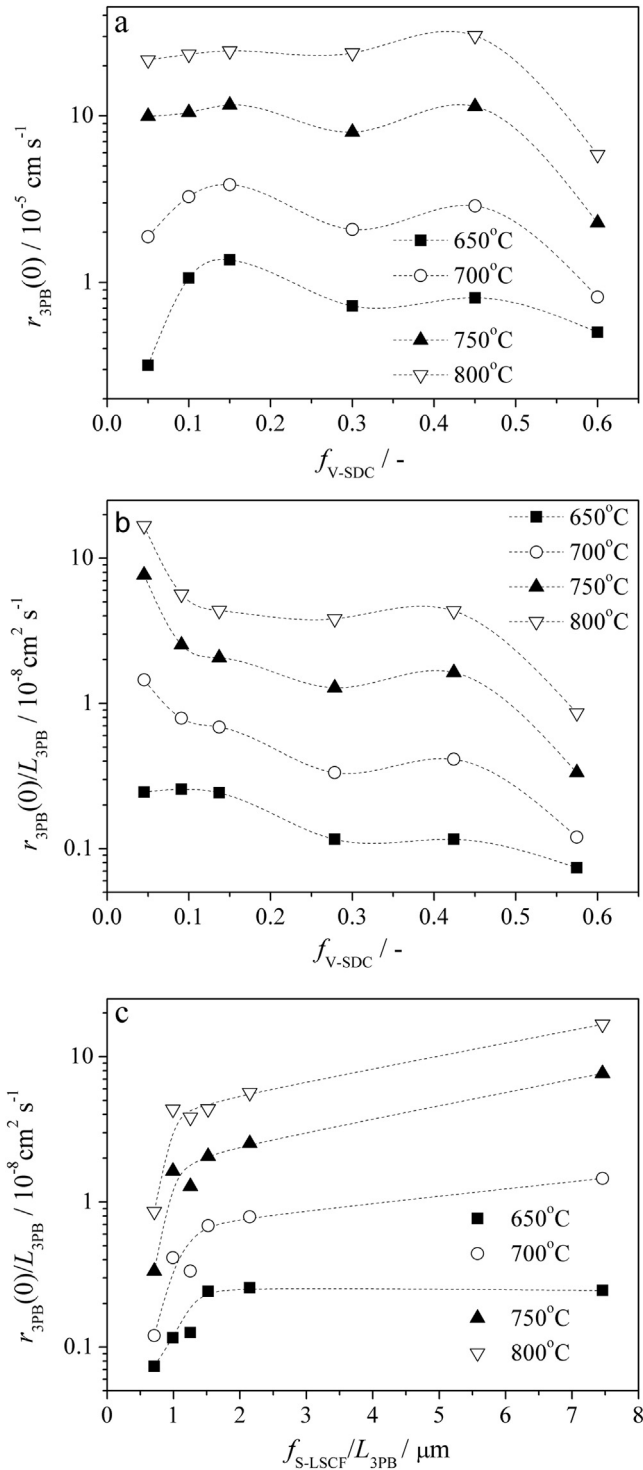


Fig. 10. a) The initial incorporation rate at 3 PB, $r_{3PB}(0)$, b) the corresponding value per unit 3 PB length, $r_{3PB}(0)/L_{3PB}$, as a function of SDC volume fraction, and c) $r_{3PB}(0)/L_{3PB}$ versus the LSCF area per unit 3 PB length, f_{S-LSCF}/L_{3PB} . Dashed lines are drawn to guide the eye.

According to the law of mass conservation, the incorporation rate per unit surface area at 3 PB can be obtained

$$r_{3PB}(t) = r_c(t) - r_{2PB,c}(t) = (k_{eff} - f_{S-LSCF}k)[1 - n_c(t)] \quad (22)$$

Eq. (22) can calculate $r_{3PB}(t)$ at anytime, including $r_{3PB}(0)$. Obviously, $r_{3PB}(t)$ is determined by the step related to oxygen vacancy from

SDC, Eq. (5). That is, $r_{3PB}(t)$ is determined by the concentration of $V_{O,SDC}''$ and $O_{ad,LSCF}''$. If it is determined only by $V_{O,SDC}''$, the reaction must be confined to the LSCF–SDC boundary, i.e. 3 PB. Since $V_{O,SDC}''$ concentration is uniform throughout SDC, $r_{3PB}(t)$ must be directly proportional to L_{3PB} . Thus, the incorporation rate per unit length of 3 PB, $r_{3PB}(0)/L_{3PB}$ ($\text{cm}^2 \text{ s}^{-1}$), should be equal for every composite. Fig. 10b shows $r_{3PB}(0)/L_{3PB}$ versus SDC volume fraction. Unfortunately, it is not a constant but seems to decrease with SDC content. This suggests that the incorporation step should not only be determined by $V_{O,SDC}''$, but also be related to $O_{ad,LSCF}''$, which is formed on the LSCF surface (Eqs. (2) and (3)) and must diffuse from the LSCF surface to the LSCF–SDC boundary. The amount of the diffused $O_{ad,LSCF}''$ should be related to the diffusion distance. The average distance for $O_{ad,LSCF}''$ to diffuse can be characterized by the LSCF area per unit length of 3 PB, f_{S-LSCF}/L_{3PB} (cm). Fig. 10c reveals $r_{3PB}(0)/L_{3PB}$ versus f_{S-LSCF}/L_{3PB} . The value of $r_{3PB}(0)/L_{3PB}$ increases rapidly with the average distance, and levels off after 1.5 μm . Fig. 10c suggests that the effective diffusion distance on the LSCF surface is about 1.5 μm . Obviously, the diffusion step dominates the oxygen incorporation at 3 PB.

3.4.2. The contribution ratio of 3 PB

The amount of incorporated oxygen per unit surface area at 3 PB can be calculated through the integral of Eq. (22)

$$h_{3PB}(t) = (k_{eff} - f_{S-LSCF}k) \int [1 - n_c(t)] dt \quad (23)$$

The total amount of incorporated oxygen per unit surface area is

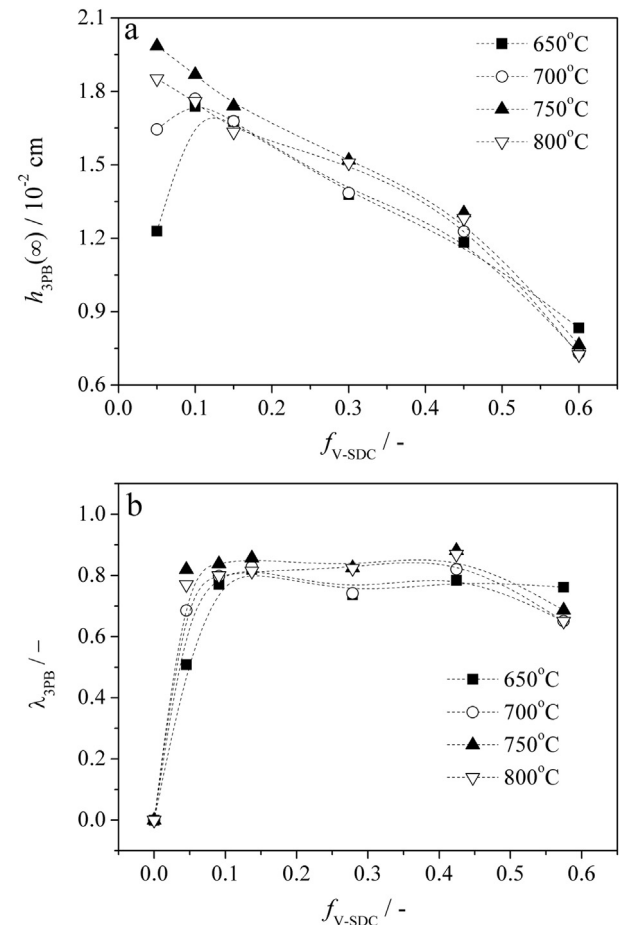


Fig. 11. a) The total amount of incorporated oxygen at 3 PB, $h_{3PB}(\infty)$, and b) the contribution ratio of 3 PB, λ_{3PB} , as a function of SDC volume fraction. Dashed lines are drawn to guide the eye.

$$h_{3PB}(\infty) = f_{V-LSCF} \frac{V}{S} \frac{k_{eff} - f_{S-LSCF}k}{k_{eff}} \quad (24)$$

Fig. 11a shows the total incorporated oxygen at 3 PB. To reflect significance of the oxygen incorporation at 3 PB, the contribution ratio, λ_{3PB} , is defined

$$\lambda_{3PB} = \frac{h_{3PB}(\infty)}{h_c(\infty)} \times 100\% = \frac{k_{eff} - f_{S-LSCF}k}{k_{eff}} \times 100\% \quad (25)$$

The contribution ratio is revealed in Fig. 11b. Obviously, 3 PB contributes the main part of exchanged oxygen, which reaches an average of over 70%. At 700 °C, it contributes about 70% when 4.5 vol. % SDC is added.

4. Conclusion

A method has been developed to precisely determine the oxygen incorporation rate and the amount of oxygen incorporated at the LSCF–SDC–gas 3 PB with the ECR technique. The effective oxygen surface exchange coefficient is defined to calculate the oxygen incorporation at 3 PB. Results surely demonstrate that oxygen incorporation at 3 PB is much more facile than that on the LSCF surface. More precisely, the 3 PB zones make the major contribution to the total oxygen incorporation, which reaches an average of over 70% even at very low volume fraction of SDC. The oxygen incorporation rate at 3 PB has been found to be not only related to the length of 3 PB but also LSCF surface area, demonstrating the reaction at 3 PB is not confined to the LSCF–SDC–gas boundary but extends to LSCF surface. The effective surface diffusion length is suggested to be 1.5 μm .

Acknowledgements

We gratefully acknowledge the financial support from the Ministry of Science and Technology of China (2012CB215403) and the National Natural Science Foundation of China (51372239).

References

- [1] V. Dusastre, J.A. Kilner, *Solid State Ionics* 126 (1999) 163–174.
- [2] E. Perry Murray, M.J. Sever, S.A. Barnett, *Solid State Ionics* 148 (2002) 27–34.
- [3] Y.J. Leng, S.H. Chan, Q.L. Liu, *Int. J. Hydrogen Energy* 33 (2008) 3808–3817.
- [4] C.J. Fu, K.N. Sun, N.Q. Zhang, X.B. Chen, D.R. Zhou, *Electrochim. Acta* 52 (2007) 4589–4594.
- [5] F. Qiang, K.N. Sun, N.Q. Zhang, X.D. Zhu, S.R. Le, D.R. Zhou, *J. Power Sources* 168 (2007) 338–345.
- [6] A.L. Shaula, V.V. Kharton, F.M.B. Marques, A.V. Kovalevsky, A.P. Viskup, E.N. Naumovich, *J. Solid State Electrochem.* 10 (2006) 28–40.
- [7] V.V. Kharton, A.V. Kovalevsky, A.P. Viskup, A.L. Shaula, F.M. Figueiredo, E.N. Naumovich, F.M.B. Marques, *Solid State Ionics* 160 (2003) 247–258.
- [8] J. Sunarso, S. Baumann, J.M. Serra, W.A. Meulenber, S. Liu, Y.S. Lin, J.C. Diniz da Costa, *J. Membr. Sci.* 320 (2008) 13–41.
- [9] S.P. Jiang, *Solid State Ionics* 146 (2002) 1–22.
- [10] J.D. Sirman, J.A. Kilner, *J. Electrochem. Soc.* 143 (1996) L229–L231.
- [11] T. Hong, L. Zhang, F.L. Chen, C.R. Xia, *J. Power Sources* 218 (2012) 254–260.
- [12] J.A. Lane, S.J. Benson, D. Waller, J.A. Kilner, *Solid State Ionics* 121 (1999) 201–208.
- [13] L. Zhao, J.J. Hyodo, K.F. Chen, N. Ai, S. Amarasinghe, T. Ishihara, S.P. Jiang, *J. Electrochem. Soc.* 160 (2013) F682–F686.
- [14] I. Yasuda, T. Hikita, *J. Electrochem. Soc.* 141 (1994) 1268–1273.
- [15] M. Kuhn, Y. Fukuda, S. Hashimoto, K. Sato, K. Yashiro, J. Mizusaki, *ECS Trans.* 35 (2011) 1881–1890.
- [16] E.N. Armstrong, K.L. Duncan, D.J. Oh, J.F. Weaver, E.D. Wachsman, *J. Electrochem. Soc.* 158 (2011) B492–B499.
- [17] A. Karthikeyan, S. Ramanathan, *Appl. Phys. Lett.* 92 (2008) 243109.
- [18] G. Kim, S. Wang, A.J. Jacobson, C.L. Chen, *Solid State Ionics* 177 (2006) 1461–1467.
- [19] H.J.M. Bouwmeester, M.W. Otter, B.A. Boukamp, *J. Solid State Electrochem.* 8 (2004) 599–605.
- [20] H. Yashiro, Y. Eguchi, K. Eguchi, H. Arai, *J. Appl. Electrochem.* 18 (1988) 527–531.
- [21] P.S. Manning, J.D. Sirman, J.A. Kilner, *Solid State Ionics* 93 (1997) 125–132.